Surface & Coatings Technology 304 (2016) 459–467

Contents lists available at ScienceDirect

Surface & Coatings Technology

journal homepage: www.elsevier.com/locate/surfcoat

Enhanced bond strength and bioactivity of interconnected 3D TiO_2 nanoporous layer on titanium implants

Ming Jin [a], Shenglian Yao [a], Lu-Ning Wang [a,*], Yi Qiao [b], Alex A. Volinsky [c]

[a] School of Materials Science and Engineering, University of Science and Technology Beijing, 100083 Beijing, China
[b] State Key Laboratory for Advanced Metals and Materials, University of Science and Technology Beijing, 100083 Beijing, China
[c] Department of Mechanical Engineering, University of South Florida, Tampa, FL 33620, USA

ARTICLE INFO

Article history:
Received 1 April 2016
Revised 13 May 2016
Accepted in revised form 15 May 2016
Available online 16 May 2016

Keywords:
Titanium
Anodization
Nanoporous
Implant

ABSTRACT

Titanium and its alloys have been extensively used as implant materials due to their excellent mechanical properties, adequate corrosion resistance and good biocompatibility. In this study, an interconnected 3D TiO_2 structure on Ti implants is fabricated via anodization method in a fluoride-containing electrolyte with water content larger than 50%. The pore size ranges from 30 to 200 nm with the current density increased from 50 to 100 $mA \cdot cm^2$. Compared with other kinds of porous TiO_2 layers, which were fabricated by the same method with different electrolyte composition, the prepared 3D TiO_2 structure shows the highest hardness and apparent Young's modulus, which are over 4 times higher than that of the TiO_2 nanotube arrays. Moreover, the 3D TiO_2 possess the highest adhesion strength as the critical load for the delamination occurred is 0.7 N, while for the nanotube-structured layer and the transition structure, the load are 0.2 and 0.4 N, respectively. Additionally, the 3D TiO_2 structure also shows better corrosion resistance than the others. Titanium with 3D oxide layer has also shown good performance in osteogenic cells culturing, since in the cell viability assay, the cells adhered on the 3D oxide layer spread extensively and showed a spindle shape while on the TiO_2 nanotube arrays or titanium with transition structure the cells were unfavorable to spread. This work can provide guidelines for improving structural and environmental conditions responsible for modification of Ti surfaces for biomedical applications.

1. Introduction

Titanium (Ti) and its alloys, occupying 40% of today's biomedical implant materials market, continue to gain increasing attention for orthopedic applications due to their excellent mechanical properties, adequate corrosion resistance and the ability to maintain their functions after being subjected to hostile environments. The initial interaction between a metal implant and a growing bone plays an important role in fabricating prostheses for load-bearing applications [1,2]. Nevertheless, a smooth and dense TiO_2 passive film on Ti metal may not impart bioactivity and chemical bonding, but is susceptible to the formation of fibrous tissues that can cause loosening of implant and induce inflammation [3]. Thus, many efforts have been put forward to improve the osseointegration of implants. Among these, implant coating with various kinds of bioactive materials is a common method [4,5]. Hydroxyapatite (HA) coating by plasma-spray technique is one of the most widely investigated methods used in clinical implants [6]. However, the difficulty of controlling the quality, composition, and crystallinity of plasma-sprayed HA coating limits their applications [7].

Adhesion of cells, such as osteoblasts, is a crucial prerequisite to cell functions, including synthesis of extracellular matrix proteins, formation of mineral deposits, and osseointegration on the substrate surface. Since the TiO_2-type nanostructures have been developed considerably, it is desired that the cells could bond with the improved and integrated structure. For example, a discrete and less continuous layer with interlock configuration and high adhesion area could minimize interface stress and delamination. Many surface treatment methods, such as the sol-gel method [8], hydrothermal methods [9], alkali coupling with heat treatment [10], physical vapor deposition (PVD) [11], and chemical vapor deposition (CVD) [12] have been used to modify the implant surfaces to promote adhesion and proliferation of cells where biomedical implants are in direct contact with tissues. Among them, etching Ti and Ti alloys surface in acidic or alkali solutions to obtain porous structure is a versatile method [13–15]. It has been reported that titanium and its alloys subjected to NaOH and heat treatment could obtain the apatite-forming capability and integrate with the living bone. The apatite-forming capability of the metal is attributed to the formation of sodium titanate on metal during the NaOH and heat treatment [13,16,17]. On the other hand, it was found that sodium-free titania with

* Corresponding author.
E-mail address: luning.wang@ustb.edu.cn (L.-N. Wang).

http://dx.doi.org/10.1016/j.surfcoat.2016.05.038
0257-8972/

specific structure of anatase and rutile possesses much higher apatite-forming ability than sodium-containing titanate in vitro [18]. Another more effective treatment has been reported as precalcification in boiling saturated $Ca(OH)_2$ solution, which is more cost-effective and safer than in NaOH [19].

Electrochemical anodization, known as anodization or anodic oxidation, is a well-established surface modification approach for metals to produce protective layers [20]. During the last several decades this method has been successfully applied for modifying orthopedic implants and has achieved some new advances in fabrication of nanostructured surfaces [21–25]. There have been numerous studies of the TiO_2 nanotubular arrays formation by anodization technique. A series of parameters, such as applied voltage [26,27], water content [28], electrolyte pH [29], and the anodization time [23], have significant effects on the topography of TiO_2 nanotubular layers. It is well accepted that not only the diameter of the tube can be accurately adjusted between 10 and 5000 nm [30], but also the nanotube layer can be easily coated on complex surfaces, such as dental-implant screws and hip implants owing to their self-organizing nature [31]. It was reported that the TiO_2 nanotubular arrays have many potential biomedical applications. Examples include bond scale and supporting platform for bone and stem cells, local delivery of antibiotics off-implant at the site of implantation, and the control of hemorrhage by forming significantly stronger clots with reduced clotting times [32–36]. Although there has been much interest in fabricating nanotubes on the surface of titanium to enhance the bioactivity of implants, few reports have commented on the interconnected three dimensional (3D) porous layers. In light of a rapid ingrowth of biomedical implants in bone, one of the key features of TiO_2 interacting with body fluids is that it stimulates hydroxyapatite growth. Moreover, a 3D structure is optimal for embedding precursors for HAp formation, which additionally promotes HAp nucleation [22]. For the nanotube structure, biocompatibility of the material with 3D porous coating could be improved. Based on its connectivity, it is believed that the three-dimensional structure would not only facilitate the circulation of body fluids, but also benefit the excretion of metabolic waste.

In this study, interconnected 3D TiO_2 structure on Ti implant via anodization in a fluoride-containing electrolyte is reported. Factors affecting the surface growth morphology are discussed along with the

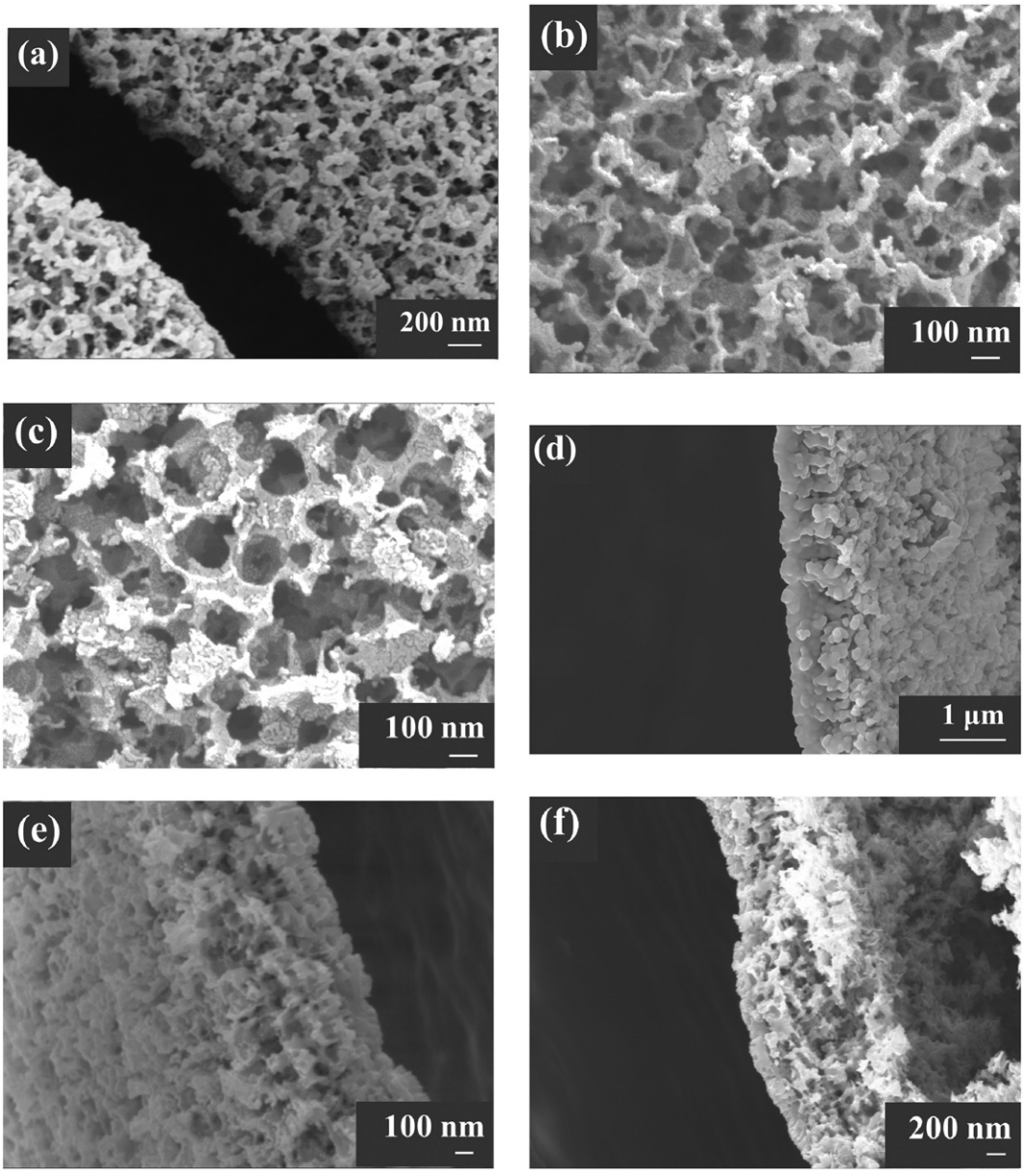

Fig. 1. Surface morphology and cross-sectional view of Ti anodized at different current densities: (a) and (d) 50 mA·cm^{-2}, (b) and (e) 80 mA·cm^{-2} and (c) and (f) 100 mA·cm^{-2}; the oxidation time is 0.5 h. The electrolyte consisted of NH_4F, H_2O and ethylene glycol; the mass ratios are 1:100:100.

properties of different surface structures. In vitro behavior of osteoblast cells cultured on different surface topography was studied, along with the effect of such diverse nanostructures on osteoblast cell morphology and cell proliferation.

2. Experiments

2.1. Specimen preparation

The sample material was Ti thin foil (99.99% pure,) with 1×1 cm^2 size and 0.25 mm thickness. Prior to anodization, the samples were ultrasonically cleaned with acetone, ethanol and deionized (DI) water, respectively, and finally dried in air. Each foil was etched in a solution containing $HF/HNO_3/H_2O$ (volume ratio, 1:4:2) for 1 s. Anodization of the metals was performed in a two-electrode configuration, where Ti foil plates were used as the working electrode and a 1.5×1.5 cm^2 platinum foil was used as the counter electrode under constant current at room temperature. A DC power supply (Maynuo M8813) was used as the current source to drive the anodization. The electrochemical experiments performed in the electrolyte consisted of NH_4F and H_2O, ethylene glycol (the mass ratios of 1:100:100, 1:40:160 and 1:20:180, respectively). The specimens were anodized for 0.5 h, and then rinsed with DI water and dried in a compressed air stream. Some of the specimens were annealed at 450 °C for 1 h with a heating rate of 5 °C·min^{-1} to convert the amorphous phase into the crystalline structure.

The mechanical properties of the coatings were probed by microindentation (Nano Indenter II) under a small depth of 100 nm. The resolution of the instrument is 75 nN, the maximum force is 700 mN and the displacement resolution of the indenter is 0.04 nm. Each reported mechanical properties value had an average of at least five measurements. Young's modulus and hardness (HV) were determined from the load-unload curves recorded during microindentation. Adhesion properties of the oxide films were characterized using Bruker CETR UMT-3 with its nanoindentation module at room temperature. A Berkevich three-sided diamond indenter was employed for the nanoscratch tests. The orientation of the Berkevich indenter tip was aligned so that the scratching could be performed in a face forward direction in order to delaminate the overcoats. A 6 mm scratching track at a constant velocity of 1 μm·s^{-1} was applied to all test samples. The indenter normal load was linearly ramped from the minimum to the maximum loads during scratching. Meanwhile, lateral force (friction force) during scratching was recorded by the system.

The SBF solution was prepared as reported by Kokubo and Takadama by dissolving reagent grade NaCl, 8.035 g, KCl, 0.225 g, $NaHCO_3$, 0.355 g, $K_2HPO_4 \cdot 3H_2O$, 0.231 g, $MgCl_2 \cdot 6H_2O$, 0.311 g, $CaCl_2$, 0.292 g, and Na_2SO_4, 0.072 g in 1 L DI water [37]. The pH of the solution was adjusted

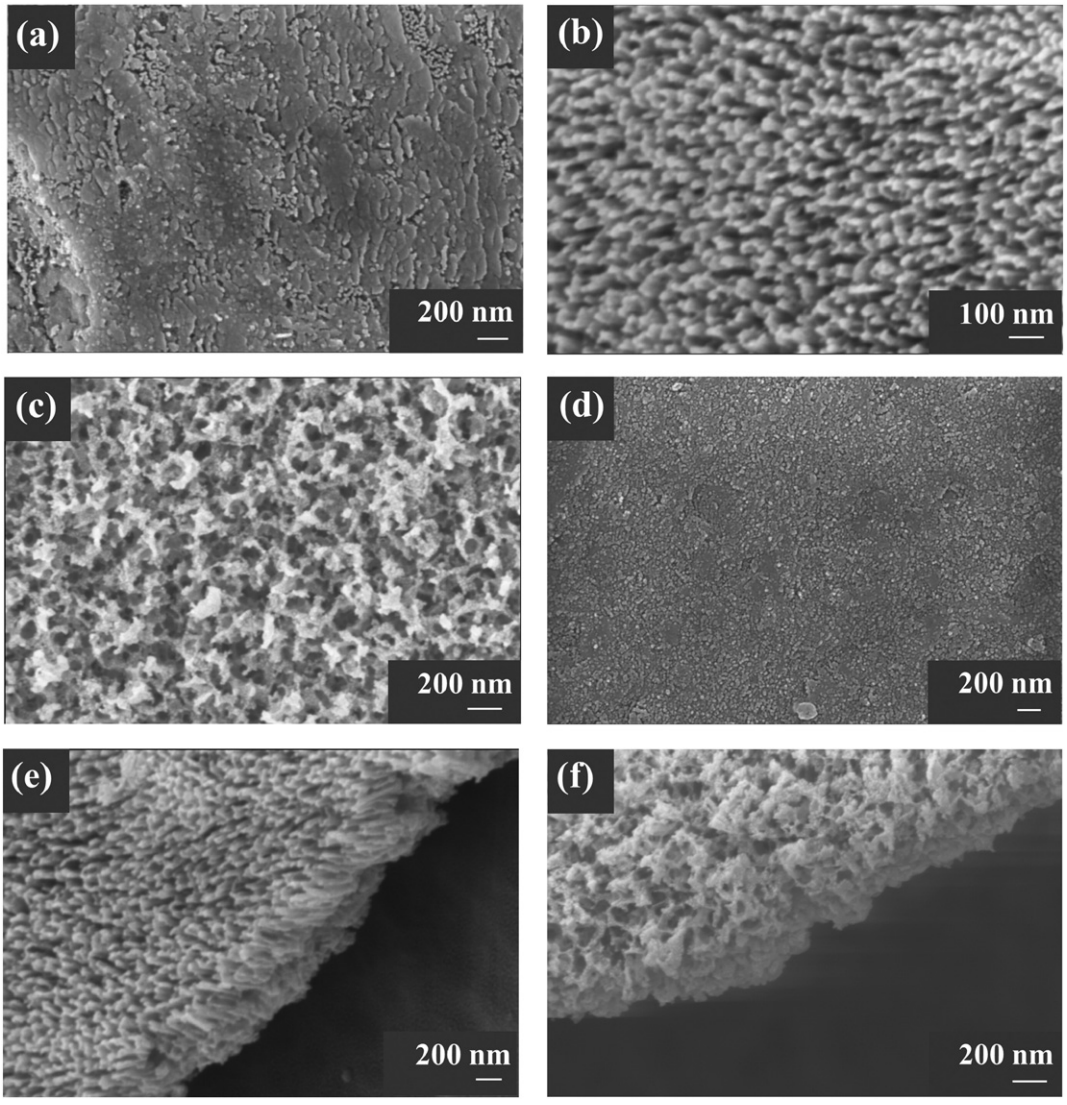

Fig. 2. Surface morphology and cross-sectional view of Ti anodized at 50 mA·cm^{-2}, the oxidation durations are (a) and (d) 10 min, (b) and (e) 20 min, (c) and (f) 30 min. The electrolyte consisted of NH_4F, H_2O and ethylene glycol; the mass ratios are 1:100:100.

to 7.4 at 37 °C by adding appropriate amounts of Tris and HCl. The setup for corrosion behavior measurements consisted of a standard three-electrode cell with a saturated calomel electrode (SCE) as a reference electrode, another electrode prepared from platinum plate as a counter electrode, and a computer controlled electrochemical workstation (CHI660E, Shanghai Chen Hua Instrument Limited Company). Open circuit potential (OCP) was recorded for 1 h at 5 s intervals after specimen immersion in SBF for 10 min. The potentiodynamic polarization behavior of the specimens was recorded after immersion for 1 h in SBF. The range of the scan was −1000 mV to +1500 mV (vs. SCE) at a scanning rate of 1 $mV \cdot s^{-1}$. The electrochemical impedance spectra (EIS) measurements were performed starting from 10^5 to 10^{-2} Hz at 10 $cycle \cdot dec^{-1}$ with an AC amplitude of ±10 mV. All tests were reproduced three times. The impedance data was analyzed with the Zview 2.70 software package and fitted to the equivalent circuits.

2.2. MC3T3-E1 cell proliferation test

MC3T3-E1 mouse clonal osteogenic cells were maintained in alpha minimum essential medium (α-MEM) supplemented with L-glutamine, 10% fetal bovine serum (FBS; Intergen, Purchase, NY, USA), 1% penicillin/streptomycin (100 IU/mL; Sigma), and streptomycin (100 $mg \cdot mL^{-1}$, Sigma). MC3T3-E1 osteoblastic cells (2×10^4 $cells \cdot well^{-1}$) were seeded onto experimental membranes in 24-well plates, and incubated at 37 °C in a humidified atmosphere with 5% CO_2.

After culturing for 1, 3, 5 and 7 days, the samples were washed by the PBS 3 times. The washed samples were cultured in α-MEM and received 1% penicillin/streptomycin and 10% FBS, 300 μL mediums and 30 μL CCK-8 solutions in a humidified incubator with 5% CO_2 at 37 °C for 3 h. Then, the 200 μL cultured solution was taken out to a 96-well culture plate. A microplate reader for enzyme linked immunosorbent assay (Bio-Rad, Hercules, CA, USA) was used to detect the OD value of the absorbance by the 450 nm wavelength. The MC3T3-E1 cell proliferation ratio of OD_a was calculated as:

$$OD_a = (OD_s - OD_b)/(OD_c - OD_b) \times 100\% \quad (1)$$

where OD_s is originated from the culture plate containing mediums, CCK-8 and samples; OD_c is originated from the culture plate containing mediums, CCK-8; and OD_b is originated from blank controls without any samples.

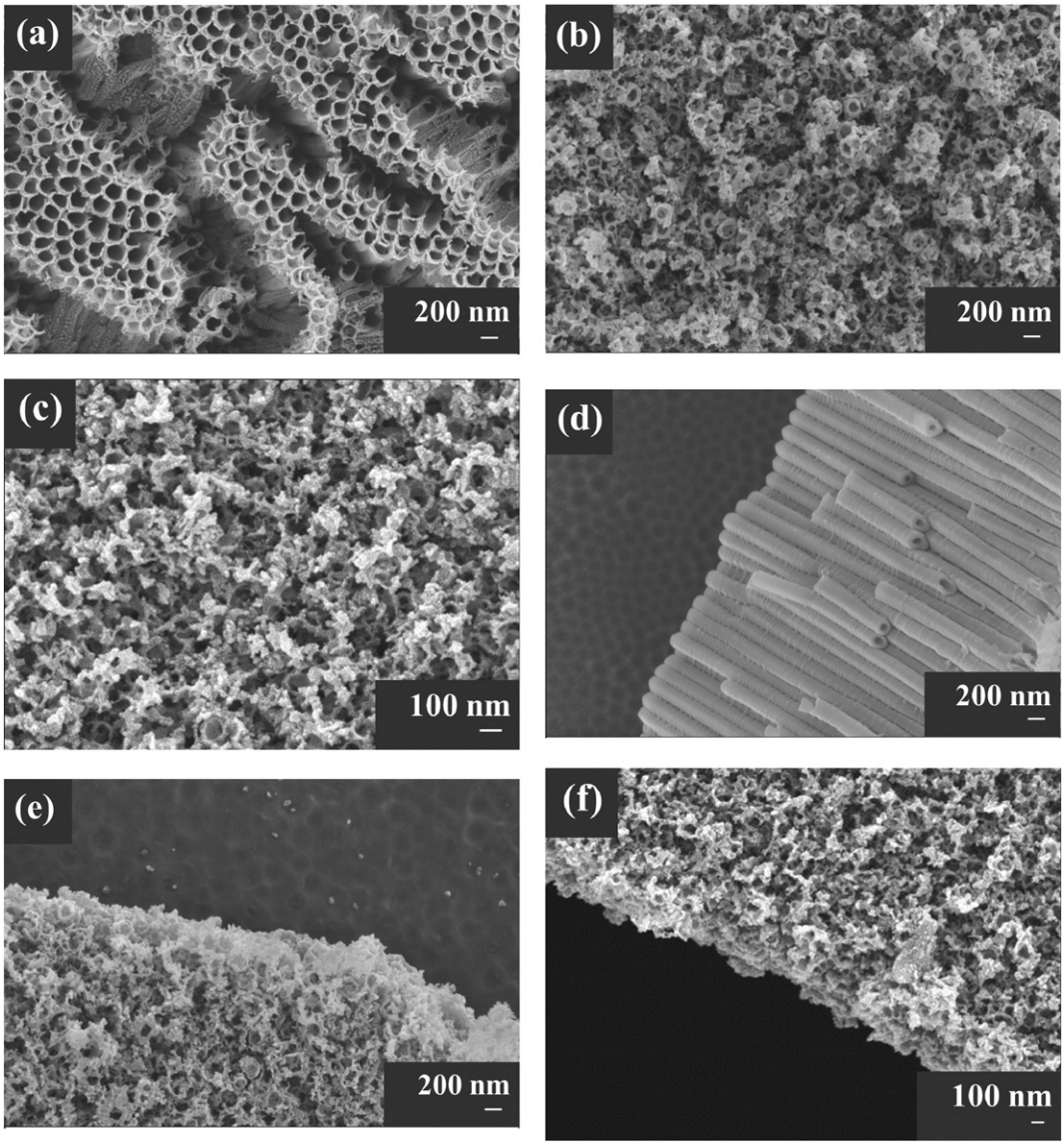

Fig. 3. Surface morphology and cross-sectional view of TiO_2 films fabricated at various electrolytes, in which the H_2O content of the electrolytes is (a) and (d) 10%, (b) and (e) 20% and (c) and (f) 50%; the anodic current density fixed at 50 $mA \cdot cm^{-2}$.

2.3. Surface morphology and crystalline structure detection

The morphology of TiO_2 morphological characterization as well as that of the adhered cells was observed using a field emission scanning electron microscope (SEM, ZEISS Auriga). For the cell observation, after the selected incubation period, the samples were washed with 0.01 M phosphate buffer solution (PBS) and distilled water, respectively, and fixed with 2.5% glutaraldehyde in 0.01 M PBS for 2 h. After fixing, they were rinsed three times with 0.01 M PBS for 10 min. The samples were then dehydrated in a graded series of alcohol (50%, 75%, 90% and 100%) for 10 min and subsequently dried by supercritical point CO_2. The dehydrated samples were sputter-coated with gold.

An X-ray diffractometer (STOFDARMSTADT, STOE/2, Cu Kα radiation) was used to examine the crystalline structure of the samples. The 2θ scanning range was 10–90° and the scanning rate was $4°\cdot min^{-1}$.

3. Results and discussion

The top and cross section morphologies of the oxides on the Ti plates anodized at 50 $mA\cdot cm^{-2}$, 80 $mA\cdot cm^{-2}$, 100 $mA\cdot cm^{-2}$ for 0.5 h are shown in Fig. 1. After anodization, titanium showed a porous structure with fine trabecular on its surface. This surface topology may play an important role in improving the bone-bonding strength of this material. The size and shape of the pores are mainly influenced by the input current density. The morphology of the oxide shown in Fig. 1a indicates that the pore sizes ranged from 30 to 90 nm when the current density was increased to 50 $mA\cdot cm^{-2}$ [38]. It was reported by Yasuda et al. [39] that the diameter of nanopore/nanotubular arrays correlates linearly with the growth factor of the transition metal oxide. The anodic oxide growth begins from a local oxide breakdown site, essentially a point source on the metal surface. From this point source the oxide growth would take place immediately in all directions leading to a hemispherical oxide structure with a certain radius $R = f_{growth}U$ (the growth factor f_{growth} being $f_{growth} = t_{film}/\Delta U$ where t_{film} being the (compact) oxide thickness that grows at a specific voltage in a valve metal). Repeated breakdown at the bottom of the pores would then lead to an oxide pore diameter proportional to the oxidation factor of the metal. Based on this assumption, the maximum pore size would increase from 90 nm to 200 nm upon increasing the output current density from 50 $mA\cdot cm^{-2}$ to 100 $mA\cdot cm^{-2}$. The cross-sectional view was taken from mechanically scratched samples, where some pieces flaked off. It can be observed that the layer thickness ranges from 1 to 2 μm.

Additionally, not only the current density, but also the anodic duration and the chemical composition of the electrolyte affect the porous structures. In the early growth stage, the growth of oxide is dominated and thus the tube is controlled by the applied field. Typically, if anodization is carried out for an extended time, tubular walls are thinned out, perforated and the tubular tops become decorated with tube wall remnants. The formation of the 3D porous structure can be deduced as below. At the beginning of electrochemical oxidation, titanium surface is entirely covered with a compact, uniform anodic oxide (Fig. 2a). The distribution of the electric field in the oxide layer, however, is strongly correlated with the surface morphological fluctuations (more pronounced fluctuations lead to more local focused electrical field). As a result, field-enhanced dissolution in the anodic oxide takes place and the pores start to form (Fig. 2b). Successively, the pore growth process reaches a steady-state and uniformly distributed pores are obtained (Fig. 2c).

In later growth stages, the process was dominated by the diffusion control [39]. Thus, the process of the growth is mainly affected by the viscosity of the electrolyte. Highest efficiency and tube lengths (hundreds of mm) can be obtained in organic viscous electrolytes, where the highest degree of ordering can also be achieved. In the present study, anodic oxidation was conducted on Ti foils and different

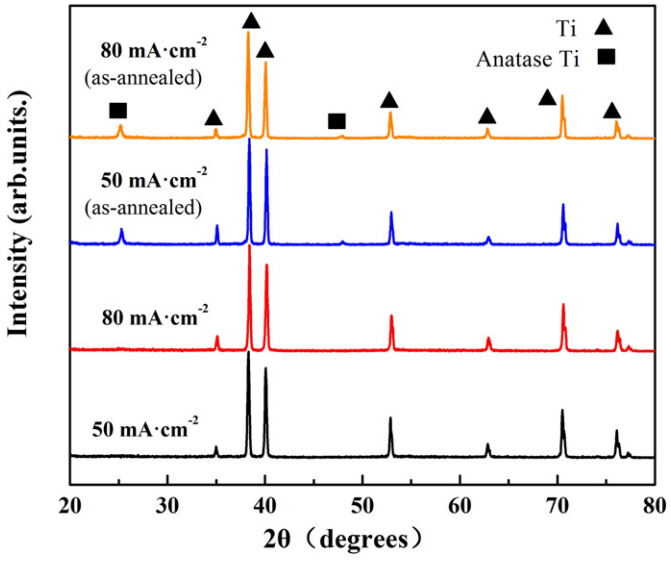

Fig. 4. XRD patterns of the titanium oxide anodized at 50 $mA\cdot cm^{-2}$, 80 $mA\cdot cm^{-2}$ before and after annealing at 450 °C.

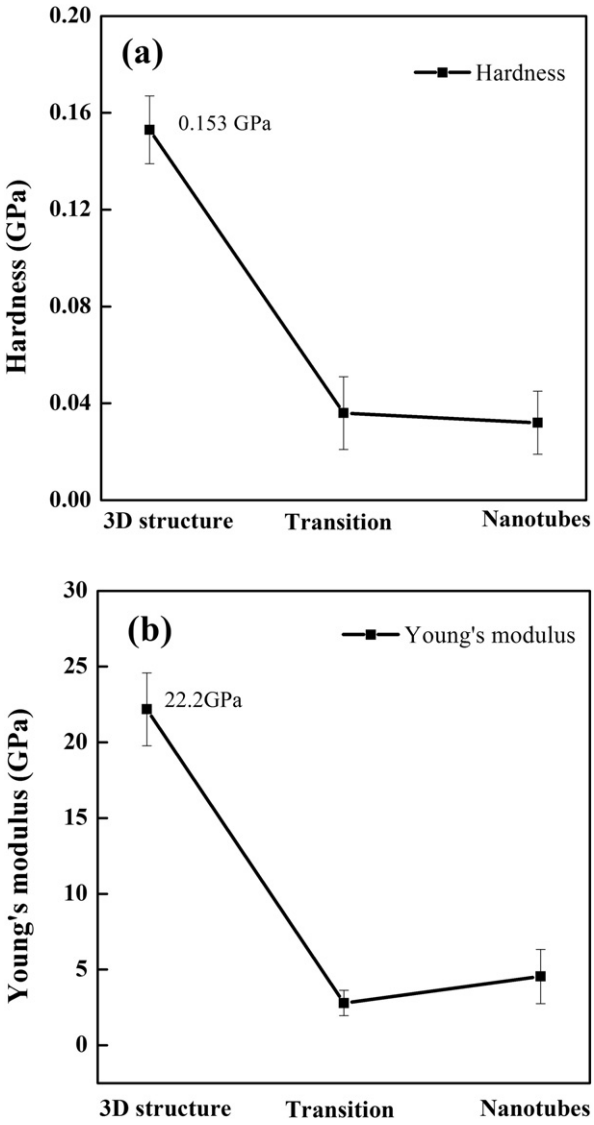

Fig. 5. Mechanical properties of TiO_2 films with different structures: (a) hardness (HV), and (b) apparent Young's modulus (Y).

morphology fabricated in electrolytes containing different amounts of water, as portrayed in Fig. 3. When the H_2O content increases to 50%, the surface morphology appears as a three dimensional structure (Ti-3D, Fig 3c). When H_2O content decreases to 10%, the surface morphology was changed to nanotube arrays (Ti-NT, Fig 3a). Further experiments showed that when the water content was 20%, the transition morphology of the structure changed from 3D to nanotube arrays, defined as the transition structure (Ti-TS, Fig 3b).

XRD patterns of the titanium oxide anodized at 50 $mA \cdot cm^{-2}$ and 80 $mA \cdot cm^{-2}$, before and after annealing at 450 °C are portrayed in Fig. 4. Since the structure of the samples before annealing is amorphous, only reflections from the titanium substrate can be observed. It is clear that after annealing the oxide is converted to the crystalline anatase phase, as shown by the squares.

Mechanical properties of TiO_2 films were evaluated via microindentation tests for obtaining information about the local hardness (HV) and the apparent Young's modulus (Y). In this study, a small depth of 100 nm was used for microindentation tests, which resulted in indentation depths smaller than 10% of the corresponding thickness of TiO_2 films, so that the influence of the substrate on the measurements of the mechanical properties of the film can be neglected [40]. As shown in Fig. 5, the oxide layer with 3D porous structure possesses the highest hardness of 0.153 GPa and apparent Young's modulus of 22.2 GPa. The corresponding values for the nanotube layer are only 0.032 GPa and 4.54 GPa, and the transition structure layer is stated in the middle. These results indicated that nanotubular arrays are softer than the Ti-3D nanoporous structure.

Delamination of an overcoat on the substrate is signaled by a sudden decrease in the applied load. The load at this position is called "the critical load", which is used to evaluate the adhesion strength between the coating and the substrate [41]. The scratch tests on the three kinds of titanium oxide layers were carried using the nanoindentor. The applied force was increased at a constant rate from 0 to 6 N. The scratch profiles are illustrated in Fig. 6. It can be seen that the critical load for the 3D structure layer is the highest (about 0.7 N), while the nanotube-structures layer possess the lowest value of 0.2 N. Thus, it can be concluded that the 3D structure has the best adhesion properties among these three samples, followed by the transition structure, and then the nanotube structure.

Fig. 7a presents curves of the open circuit potential (OCP) with respect to soaking time for Ti-NT, Ti-3D and Ti-TS samples. The OCP curves portrayed in Fig. 7a showed that all the potentials shifted positively, which indicated that all the surfaces reached a relatively stable state after the samples were immersed in SBF for 1 h. The OCP values after 1 h stabilization in SBF for three kinds of samples showed the following sequence: Ti-TS (274 ± 23 mV) > Ti-3D (200 ± 6 mV) > Ti-NT (81 ± 30 mV). The OCP values for Ti-TS and Ti-3D were better than Ti-3D samples, implying better corrosion resistance properties. Fig. 7b depicts the potentiodynamic curves for three different samples in SBF. Among them, Ti-3D and Ti-TS has higher corrosion potential than Ti-NT. The

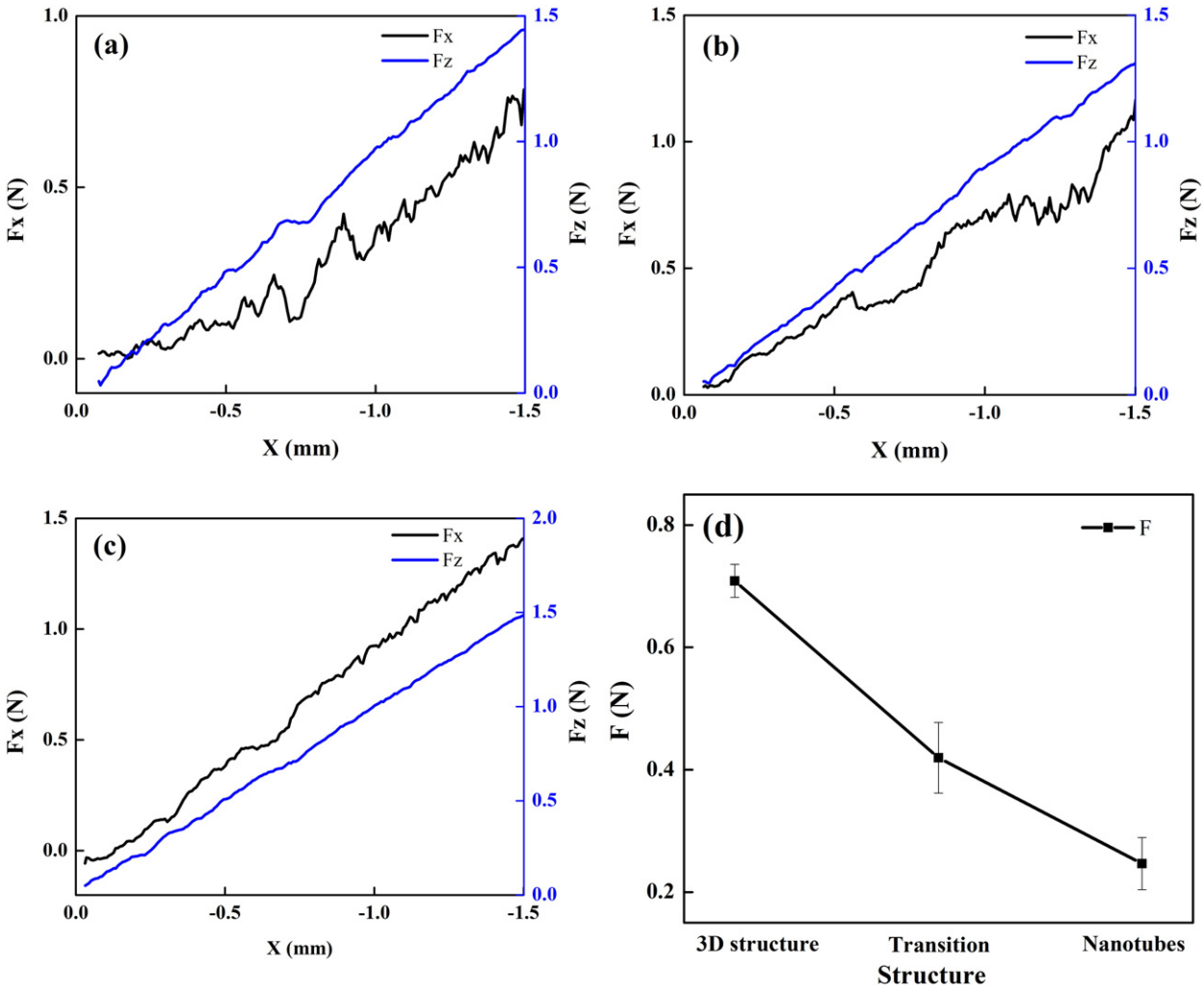

Fig. 6. The scratch tests on the three kinds of titanium oxide layers, (a) Ti-3D; (b) Ti-TS; (c) Ti-NT; Critical loads were labeled by the cycles and plotted in (d).

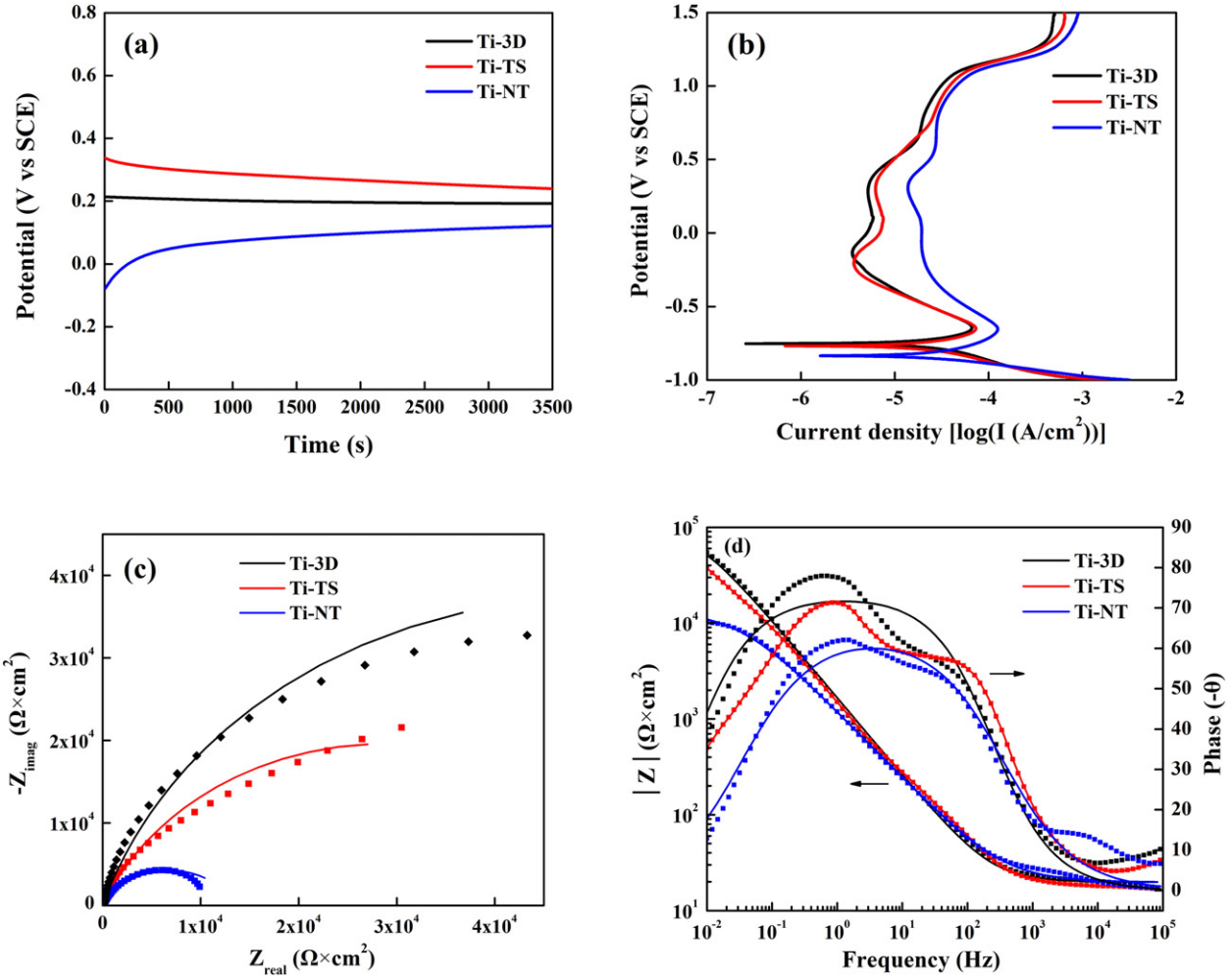

Fig. 7. (a) OCP versus immersion time; (b) potentiodynamic polarization curves; (c) Nyquist diagrams, (d) Bode diagrams of Ti-3D, Ti-TS and Ti-NT samples in SBF and (e) the equivalent circuit to model the impedance spectra of the samples.

corrosion potential of the three samples was in the order of Ti-3D ≈ Ti-TS > Ti-NT. Table 1 summarizes all the corrosion parameters obtained from OCP and potentiodynamic tests for the three materials. The corrosion current density of the three samples was about the same. Fig. 7c portrays the Nyquist plots of the three materials. Spectra show that Ti-3D had the greatest impedance. One can see the corresponding frequency of the impedance spectra of the three samples. The impedance of Ti-3D was higher than that of Ti-TS and Ti-NT, reflecting better corrosion resistance, which is consistent with the potential tested by electrochemical measurements. Fig. 7d shows the Bode impedance spectra obtained from the three materials. The order of impedance values is Ti-3D > Ti-TS > Ti-NT. The impedance spectra were fitted using the ZView 2.70 software to obtain the equivalent circuits. The spectra obtained from the samples were interpreted using one time constant composed with R_s (R_1 and CPE), where R_s is the series resistance, R_1 is the sample resistance and CPE represents the constant phase element, as shown in Fig. 7e. The electrochemical parameters obtained by fitting the circuits (error of less than 10%) are presented in Table 2. The values of R_1 indicate that the Ti-3D had a higher value than Ti-TS and Ti-NT. Results from the EIS spectra and fitting parameters from the equivalent circuits are in agreement with the results obtained from potentiodynamic tests.

Osteoblast cells play a critical role in the early stages of osseointegration. Of the different cellular models, the osteogenic cell line MC3T3-E1 is one of the most widely used. It has been shown that this non-transformed cell line expresses high ALP activity with mineralization of the extracellular matrix in vitro [42,43]. This cell line is thus a good candidate for studying the cell adhesion, proliferation and differentiation of osteoblasts on titanium surfaces. Several in vitro studies have primarily investigated the effects of surface roughness on the adhesion, proliferation and differentiation of osteoblastic cells. In general, cells cultured on rougher surfaces tended to exhibit attributes of more differentiated osteoblasts than the cells cultured on smoother surfaces for comparable periods of time, e.g. reduced cell numbers and generally

Table 1
Electrochemical parameters obtained from OCP and potentiodynamic polarization test.

Material	E_{ocp} (mV)	E_{corr} (mV)	I_{corr} (μA·cm^{-2})
Ti-3D	274 ± 23	−754 ± 16	27 ± 7
Ti-TS	200 ± 6	−761 ± 21	32 ± 5
Ti-NT	81 ± 30	−831 ± 9	48 ± 11

Table 2
Fitted electrochemical parameters determined from the Bode spectra based on the equivalent circuits.

Material	R_s (Ω)	R_1 (Ω)	CPE T-1	CPE P-2
Ti-3D	19.84 ± 1.87	$1.18 \pm 0.29 \times 10^5$	$1.35 \pm 0.16 \times 10^{-4}$	0.81 ± 0.09
Ti-TS	17.09 ± 3.09	$5.78 \pm 2.67 \times 10^4$	$1.55 \pm 0.34 \times 10^{-4}$	0.76 ± 0.21
Ti-NT	19.76 ± 2.36	$1.36 \pm 0.35 \times 10^4$	$2.22 \pm 0.24 \times 10^{-5}$	0.71 ± 0.14

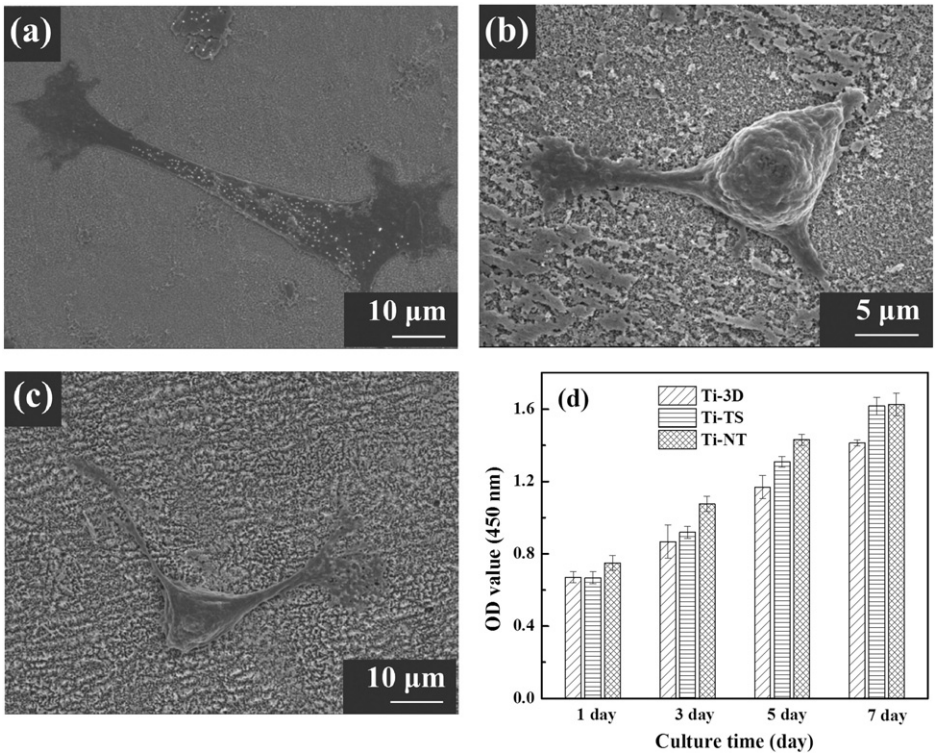

Fig. 8. Typical SEM morphology of the MC3T3-E1 cells adhering to the surfaces of (a) Ti-3D; (b) Ti-TS; (c) Ti-NT; (d) proliferation of the MC3T3-E1 cells on the different TiO_2 films.

increased alkaline phosphate-specific activity [44]. These in vitro results were related to higher implant survival rates in clinical practice for roughened implants, compared with machined surfaces [45]. In the present study, titanium surfaces were prepared and analyzed using advanced techniques prior to investigating osteoblastic cell behavior. Cell culture results obtained on a three dimension surface were compared with results from the transition structure surface and the nanotube surface. The cell viability assay indicated that all surfaces were cytocompatible (Fig. 8d). This is in agreement with the numerous studies indicating that titanium is a biocompatible substrate for cell culturing [46]. After 7 days, the attached cells were observed by SEM, as shown in Fig. 8a–c. The cells adhere tightly to the substrates with dense filopodias. Fig. 8a reveals that the cells on Ti-3D spread extensively and have a spindle shape, as Ti-3D is the best sample for cells adhesion, whereas Ti-TS and Ti-NT are more unfavorable to the spreading of cells for the adherent cells.

4. Conclusions

In this study, an interconnected 3D TiO_2 structure along with nanotube array and transition structure on Ti implant were constructed via anodization in a fluoride-containing electrolyte. The size and shape of the pores are mainly influenced by the input current density, the time used and the water content of the electrolyte. The mechanical properties revealed that the 3D structure oxide layer possesses the highest hardness, apparent Young's modulus and adhesion strength, while the nanotube array shows the lowest value. The electrochemical test indicated that 3D structure oxide layers have better corrosion resistance properties compared with nanotubular layers. Based on the special structure, titanium with 3D oxide layer has shown good performance in the osteogenic cell culturing.

Acknowledgements

This work was conducted under contract No. YETP0419 from the Beijing Higher Education Young Elite Teacher Project, No. 51501008 and No. U1560103 from the National Natural Science Foundation of China.

References

[1] B. Feng, J. Weng, B.C. Yang, S.X. Qu, X.D. Zhang, Characterization of surface oxide films on titanium and adhesion of osteoblast, Biomaterials 24 (2003) 4663–4670.
[2] D.A. Puleo, L.A. Holleran, R.H. Doremus, R. Bizios, Osteoblast responses to orthopedic implant materials in vitro, J. Biomed. Mater. Res. 25 (1991) 711–723.
[3] O.V. Salata, Applications of nanoparticles in biology and medicine, J. Nanobiotechnol. 2 (2004) 3–9.
[4] K. Takatsuka, T. Yamamuro, T. Kitsugi, T. Nakamura, T. Shibuya, T. Goto, A new bioactive glass–ceramic as a coating material on titanium alloy, J. Appl. Biomater. 4 (1993) 317–329.
[5] T. Kitsugi, T. Nakamura, M. Oka, Y. Senaha, T. Goto, T. Shibuya, Bone-bonding behavior of plasma-sprayed coatings of Bioglass, AW-glass ceramic, and tricalcium phosphate on titanium alloy, J. Biomed. Mater. Res. 30 (1996) 261–269.
[6] K. Duan, R. Wang, Surface modifications of bone implants through wet chemistry, J. Mater. Chem. 16 (2006) 2309–2321.
[7] R.B. Heimann, H.V. Tran, P. Hartmann, Laser-Raman and nuclear magnetic resonance (NMR) studies on plasma-sprayed hydroxylapatite coatings: influence of bioinert bond coats on phase composition and resorption kinetics in simulated body fluid, Mater. Werkst. 34 (2003) 1163–1169.
[8] P. Li, K. De Groot, T. Kokubo, Bioactive $Ca_{10}(PO_4)_6(OH)_2-TiO_2$ composite coating prepared by sol-gel process, J. Sol-Gel Sci. Technol. 7 (1996) 27–34.
[9] Y. Suzuki, S. Yoshikawa, Synthesis and thermal analyses of TiO2-derived nanotubes prepared by the hydrothermal method, J. Mater. Res. 19 (2004) 982–985.
[10] X.J. Wang, Y.C. Li, J.G. Lin, P.D. Hodgson, C.E. Wen, Apatite-inducing ability of titanium oxide layer on titanium surface: the effect of surface energy, J. Mater. Res. 23 (2011) 1682–1688.
[11] V. Karagkiozaki, S. Logothetidis, N. Kalfagiannis, S. Lousinian, G. Giannoglou, Atomic force microscopy probing platelet activation behavior on titanium nitride nanocoatings for biomedical applications, Nanomed.: Nanotechnol., Biol. Med. 5 (2009) 64–72.
[12] C. Saulou, B. Despax, P. Raynaud, S. Zanna, P. Marcus, M. Mercier-Bonin, Plasma deposition of organosilicon polymer thin films with embedded nanosilver for prevention of microbial adhesion, Appl. Surf. Sci. 256 (S35-S9) (2009).
[13] H.M. Kim, F. Miyaji, T. Kokubo, T. Nakamura, Preparation of bioactive Ti and its alloys via simple chemical surface treatment, J. Biomed. Mater. Res. 32 (1996) 409–417.
[14] H. Wen, J. De Wijn, F. Cui, K. De Groot, Preparation of bioactive Ti6Al4V surfaces by a simple method, Biomaterials 19 (1998) 215–221.
[15] D.K. Pattanayak, T. Kawai, T. Matsushita, H. Takadama, T. Nakamura, T. Kokubo, Effect of HCl concentrations on apatite-forming ability of NaOH-HCl- and heat-treated titanium metal, J. Mater. Sci. Mater. Med. 20 (2009) 2401–2411.

[16] H. Kim, F. Miyaji, T. Kokubo, T. Nakamura, Effect of heat treatment on apatite-forming ability of Ti metal induced by alkali treatment, J. Mater. Sci. Mater. Med. 8 (1997) 341–347.
[17] H.M. Kim, F. Miyaji, T. Kokubo, S. Nishiguchi, T. Nakamura, Graded surface structure of bioactive titanium prepared by chemical treatment, J. Biomed. Mater. Res. 45 (1999) 100–107.
[18] M. Uchida, H. Kim, T. Kokubo, N. T., Apatite-forming ability of titania gels with different structures, Bioceramics-Conference: World Scientific 1999, pp. 149–152.
[19] B. Feng, J. Chen, S. Qi, L. He, J. Zhao, X. Zhang, Carbonate apatite coating on titanium induced rapidly by precalcification, Biomaterials 23 (2002) 173–179.
[20] C. Yao, T.J. Webster, Anodization: a promising nano-modification technique of titanium implants for orthopedic applications, J. Nanosci. Nanotechnol. 6 (2006) 2682–2692.
[21] A. Ghicov, P. Schmuki, Self-ordering electrochemistry: a review on growth and functionality of TiO_2 nanotubes and other self-aligned MO(x) structures, Chem. Commun. 2791-808 (2009).
[22] P. Roy, S. Berger, S. P., TiO_2 nanotubes: synthesis and applications, Angew. Chem. 50 (2011) 2904–2939.
[23] S.P. Albu, A. Ghicov, J.M. Macak, P. Schmuki, 250 μm long anodic TiO_2 nanotubes with hexagonal self-ordering, Phys. Status Solidi Rapid Res. Lett. 1 (R65-R7) (2007).
[24] J.M. Macak, H. Tsuchiya, P. Schmuki, High-aspect-ratio TiO_2 nanotubes by anodization of titanium, Angew. Chem. 44 (2005) 2100–2102.
[25] S. Bauer, S. Kleber, S. P., TiO_2 nanotubes: tailoring the geometry in H3PO4/HF electrolytes, Electrochem. Commun. 8 (2006) 1321–1325.
[26] K. Yasuda, P. Schmuki, Control of morphology and composition of self-organized zirconium titanate nanotubes formed in $(NH_4)_2SO_4/NH_4F$ electrolytes, Electrochim. Acta 52 (2007) 4053–4061.
[27] W. Chanmanee, A. Watcharenwong, C.R. Chenthamarakshan, P. Kajitvichyanukul, N.R. de Tacconi, K. Rajeshwar, Formation and characterization of self-organized TiO_2 nanotube arrays by pulse anodization, J. Am. Chem. Soc. 130 (2008) 965–974.
[28] J.M. Macak, H. Tsuchiya, L. Taveira, S. Aldabergerova, P. Schmuki, Smooth anodic TiO_2 nanotubes, Angew. Chem. 44 (2005) 7463–7465.
[29] S. So, K. Lee, P. Schmuki, Ultrafast growth of highly ordered anodic TiO_2 nanotubes in lactic acid electrolytes, J. Am. Chem. Soc. 134 (2012) 11316–11318.
[30] L.N. Wang, M. Jin, Y. Zheng, Y. Guan, X. Lu, J.L. Luo, Nanotubular surface modification of metallic implants via electrochemical anodization technique, Int. J. Nanomedicine 9 (2014) 4421–4435.
[31] C. von Wilmowsky, S. Bauer, R. Lutz, M. Meisel, F.W. Neukam, T. Toyoshima, et al., In vivo evaluation of anodic TiO_2 nanotubes: an experimental study in the pig, J. Biomed. Mater. Res. B Appl. Biomater. 89 (2009) 165–171.
[32] S. Oh, K.S. Brammer, Y.S. Li, D. Teng, A.J. Engler, S. Chien, et al., Stem cell fate dictated solely by altered nanotube dimension, Proc. Natl. Acad. Sci. U. S. A. 106 (2009) 2130–2135.
[33] J. Park, S. Bauer, K.A. Schlegel, F.W. Neukam, K. von der Mark, S. P., TiO_2 nanotube surfaces: 15 nm–an optimal length scale of surface topography for cell adhesion and differentiation, Small 5 (2009) 666–671.
[34] Y.-Y. Song, F. Schmidt-Stein, S. Bauer, P. Schmuki, Amphiphilic TiO_2 nanotube arrays: an actively controllable drug delivery system, J. Am. Chem. Soc. 131 (2009) 4230–4232.
[35] S.C. Roy, M. Paulose, C.A. Grimes, The effect of TiO_2 nanotubes in the enhancement of blood clotting for the control of hemorrhage, Biomaterials 28 (2007) 4667–4672.
[36] L.-N. Wang, Enhancement of hydroxyapatite formation on anodic TiO_2 nanotubular arrays via precalcification, J. Porous. Mater. 20 (2012) 183–190.
[37] T. Kokubo, H. Takadama, How useful is SBF in predicting *in vivo* bone bioactivity? Biomaterials 27 (2006) 2907–2915.
[38] L.V. Taveira, J.M. Macak, K. Sirotna, L.F.P. Dick, P. Schmuki, Voltage oscillations and morphology during the galvanostatic formation of self-organized TiO_2 nanotubes, J. Electrochem. Soc. 153 (2006) B137–B143.
[39] K. Yasuda, J.M. Macak, S. Berger, A. Ghicov, P. Schmuki, Mechanistic aspects of the self-organization process for oxide nanotube formation on valve metals, J. Electrochem. Soc. 154 (2007) C472–C478.
[40] X. Tang, D. Li, Fabrication, geometry, and mechanical properties of highly ordered TiO_2 nanotubular arrays, J. Phys. Chem. C 113 (2009) 7107–7113.
[41] H. Deng, T.W. Scharf, J.A. Barnard, Adhesion assessment of silicon carbide, carbon, and carbon nitride ultrathin overcoats by nanoscratch techniques, J. Appl. Phys. 81 (1997) 5396–5398.
[42] H. Sudo, H.-A. Kodama, Y. Amagai, S. Yamamoto, S. Kasai, In vitro differentiation and calcification in a new clonal osteogenic cell line derived from newborn mouse calvaria, J. Cell Biol. 96 (1983) 191–198.
[43] L. Le Guehennec, M.A. Lopez-Heredia, B. Enkel, P. Weiss, Y. Amouriq, P. Layrolle, Osteoblastic cell behaviour on different titanium implant surfaces, Acta Biomater. 4 (2008) 535–543.
[44] M. Bachle, R.J. Kohal, A systematic review of the influence of different titanium surfaces on proliferation, differentiation and protein synthesis of osteoblast-like MG63 cells, Clin. Oral Implants Res. 15 (2004) 683–692.
[45] T. Albrektsson, A. Wennerberg, Oral implant surfaces: part 2–review focusing on clinical knowledge of different surfaces, Int. J. Prosthodont. 17 (2003) 544–564.
[46] M. Schuler, D. Trentin, M. Textor, S.G. Tosatti, Biomedical interfaces: titanium surface technology for implants and cell carriers, Future Med. 1 (2006) 449–463.